PCCP

Accepted Manuscript

ROYAL SOCIETY OF CHEMISTRY

www.rsc.org/pccp

Cite this: DOI: 10.1039/c0xx00000x

www.rsc.org/xxxxxx

ARTICLE TYPE

Chemical induced porosity on $BiVO_4$ films produced by double magnetron sputtering to enhance the photo-electrochemical response

Sitaramanjaneya Mouli Thalluri, [a,*] Roberto Mirabal Rojas,[b] Osmary Depablos Rivera,[b] Simelys Hernández,[a,c] Nunzio Russo [a] and Sandra Elizabeth Rodil [b]

Received (in XXX, XXX) XthXXXXXXXXX 20XX, Accepted Xth XXXXXXXXX 20XX
DOI: 10.1039/b000000x

Double magnetron sputtering (DMS) is an efficient system that is well known because of its precise control of the thin film synthesizing process over any kind of substrate. Here, DMS has been adopted to synthesize $BiVO_4$ films over a conducting substrate (FTO), using metallic Vanadium and ceramic Bi_2O_3 targets simultaneously. The films were characterized using different techniques, such as X-ray diffraction (XRD), UV-Vis spectroscopy, Raman spectroscopy, X-ray photoelectron spectroscopy (XPS), field emission scanning electron microscopy (FESEM) and Profilometry. The photo-electrochemical analysis was performed by linear scan voltammetry, chrono-amperometry and electrochemical impedance spectroscopy (EIS) under the illumination of simulated solar light at 1sun. The photocurrent density of the sputtered $BiVO_4$ thin films could be improved from 0.01 mA/cm^2 to 1.19 mA/cm^2 at 1.23 V *vs* RHE by a chemical treatment using potassium hydroxide (KOH). The effect of KOH was the removal of impurities in the grain boundaries, leading to a more porous structure and more pure crystalline monoclinic $BiVO_4$ particles. Such variations in the microstructure as well as the improvement on the charge transfer properties of the $BiVO_4$ film after the KOH treatment were confirmed and deeply studied by EIS analysis.

Introduction

Water oxidation is a process that is considered to be one of the most difficult and important reactions, in view of the end products and their application in diverse fields.[1] Moreover, the use of the visible light portion of sunlight for the water oxidation process is another challenge that requires the development of new materials[2] to function as photo-anodes. Among the different metal oxide semiconductors that are available, $BiVO_4$ has been proved to be one of the most interesting materials for this reaction.[3-5]

$BiVO_4$ is a metal oxide semiconductor that has a suitable band gap position for the water oxidation process.[6] Its band gap is considered to be between 2.3 and 2.8 eV, which is the energy associated to the visible region of the solar spectrum. $BiVO_4$ occurs in three phases: monoclinic scheelite, tetragonal scheelite and tetragonal zircon. Comparatively, monoclinic scheelite $BiVO_4$ is considered as the most photoactive phase, as it shows higher ability to oxidize water into O_2.[4]

Synthesizing a photo-anode using $BiVO_4$ is a challenging task.[7] A successful photo-anode should have the following properties in order to have a good activity: high-energy conversion efficiency, high stability, low-cost production, and simple structure for the effective utilization of the photo-anode area.[8] In this context, there are a number of procedures that can be employed to synthesize $BiVO_4$ photo-anodes, and some of them have been shown to be successful in reaching the above-required characteristics of a thin film.[4] Photo-anodes of $BiVO_4$ have been prepared using $BiVO_4$ powders,[9] solutions,[10-14] and directly employing precursor materials.[15, 16]

Recently, thin $BiVO_4$ photo-anode films have been synthesized from inorganic precursors, through chemical vapor deposition [15, 17] and physical vapor deposition (PVD).[16, 18] Among the PVD methods, magnetron sputtering is a scalable technique that is widely used in industry for the synthesis of thin films of various materials on different substrates. In this paper, the dual magnetron sputtering (DMS), method has been used for the synthesis of thin $BiVO_4$ films. Chen *et al.* have reported the production of $BiVO_4$ thin films by DMS using the same target configuration. The photocurrent achieved for the pure $BiVO_4$ films was 0.5 mA/cm.[2,16] Further improvement was achieved after addition of WO_3 layers or Mo doping.[19] In the present paper, we show that it is also possible to improve the photocurrent of sputtered $BiVO_4$ by a simple chemical treatment using potassium hydroxide (KOH). The effect of the KOH treatment on the composition, microstructure, optical properties and electrochemical response is presented. DMS can be considered very important in this field, since the same process could also be used to improve the performance of thin films through various modifications, such as doping,[20] co-catalyst addition [21, 22] or hetero junction formation.[23]

Materials and Methods

a) Double magnetron sputtering deposition of $BiVO_4$ films

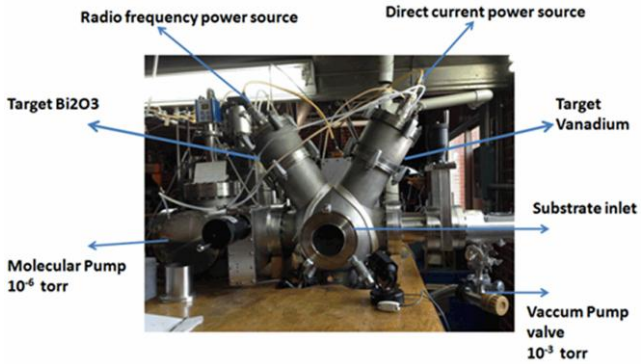

Fig.1 Double magnetron sputtering chamber

The employed DMS chamber is described in Figure 1. In order to investigate the effects of the chemical composition on the electrical and optical properties, $BiVO_4$ films were deposited using reactive magnetron sputtering under different conditions, and the best condition was chosen for a more detailed investigation. The magnetron sputtering system was equipped with two confocal planar magnetron sources, with their axes positioned at about 25° or 30° off the vertical (Bi_2O_3 (99.999 *At. %*) and V (99.95 *At. %*)), while the substrate-target distance was fixed at 100 mm to avoid angular deposition effects. The substrates were mounted onto a rotary sample holder manipulator in order to guarantee film homogeneity. The deposition chamber was connected to a turbo molecular pump through an adaptive pressure controller valve, which allowed the final total pressure in the sputtering chamber to be fixed. Mass flow regulators were fitted to control the sputtering Ar and O_2 gases independently. The target diameters were 5 cm in both cases. Before the deposition of the films, the residual pressure in the sputtering chamber was 10^{-6} Torr. Initially, different deposition conditions were considered; the power applied to the targets, the substrate temperature and the Ar/O_2 flow ratios were varied. The structural characterization using X-ray diffraction including high temperature analysis made it possible to select the conditions to obtain the monoclinic phase. Previous results in the literature of $BiVO_4$ films made by DMS indicated that such a phase could only be produced after thermal annealing (about 500 °C) of the samples in air.[16] However, we used a lower annealing temperature (400 °C) since the in-situ annealing XRD analysis demonstrated that the monoclinic phase was already formed at 300 °C as observed in Figure S1 (S.I). Moreover, a KOH chemical treatment (1M for 20 min) was also used in order to improve the photocurrent density. The conditions reported here correspond to a high DC power of 165 W applied to the V target, and an RF power of 30 W applied to the Bi_2O_3 target for a period of 25 min. The substrate temperature was kept constant at room temperature, and the total working pressure, $P_T = (P_{Ar} + P_{O2})$, was fixed at 5 x 10^{-3} torr using an O_2/Ar flow ratio of 2/18.

b) Thin films characterization

The samples were characterized using the following instruments: the diffraction patterns were obtained before and after annealing using a Rigaku Ultima IV system with Thin Film mode attachment, but using the Bragg–Brentano configuration equipped with *Cu* K_α radiation (λ = *1.5418 A*°) and a chamber for in-situ programmed temperature analysis; the Raman characterization was performed using En-Spectra R532, an Enhanced Spectroscopy instrument equipped with an Olympus CX41 Microscope system with a Green laser (532 nm wavelength); the UV-Vis absorption spectra were recorded in transmittance mode on a UV-Vis Varian Cary 5000 spectrophotometer; the morphology of the samples was investigated by means of field emission scanning electron microscopy (FESEM), using an FE-SEM MERLIN ZEISS, equipped with an energy dispersive analysis system (EDS), which was employed to obtain insight into the bulk elemental composition of the sample; thickness measurements were conducted using a DEKTAK profilometer on a step intentionally left for such purposes. The XPS analyses were carried out with a VG Escalab 200-C X-ray photo-electron-spectrometer with a non-monochromatic Mg-K source. Pass energy of 20 eV, a resolution of 1.1 eV, and a step of 0.2eV were used for high-resolution spectra.

c) Photoelectrochemical tests

Photo-electrochemical characterizations of the $BiVO_4$ electrodes were carried out in an aqueous 0.1M Na_2SO_4 electrolyte solution (*pH*~ 6.2), employing a multi-channel VSP potentiostat/galvanostat made by BioLogic. A three-electrode system, consisting of the $BiVO_4$ material as the working electrode, a platinum counter electrode and an Ag/AgCl (3M) as the reference electrode, was used. Linear scan voltammetries (LSVs) were performed in the dark and under simulated solar light, using a 450 W Xe lamp by Newport with an AM 1.5 filter and a water filter. The intensity of the light was maintained at 100 mW cm^{-2} by adjusting the distance between the source and the photo-electrochemical cell (PEC). Chrono-amperometry (*I-t*) measurements were performed at 0.6 V *vs* Ag/AgCl over continuous ON-OFF light cycles. Electrochemical Impedance Spectroscopy (EIS) measurements were conducted in the 100 mHz to 1 MHz frequency range, with an amplitude of 25 mV, under an applied DC potential of 0.6 V *vs* Ag/AgCl, under the above reported simulated sun-light condition. The EIS data were modeled using an EIS analyzer (Open source).[24] The electrochemical data presented in the work refer to the reversible hydrogen electrode (RHE) potential, calculated with $E_{RHE} = E_{Ag/AgCl} + 0.209\ V + 0.059 \cdot pH$.

Results and discussion

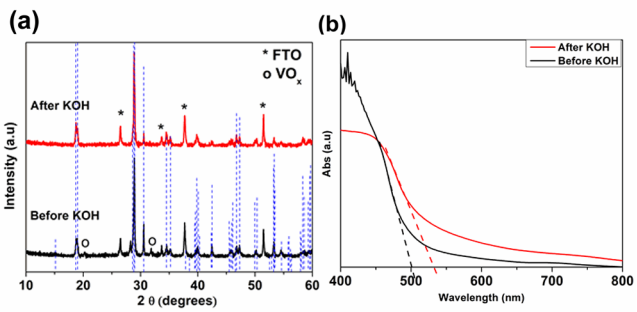

Fig 2 (a) XRD patterns (b) UV-Vis absorption spectra of $BiVO_4$ films before and after the KOH treatment

The thin $BiVO_4$ films were successfully synthesized employing the DMS method. The structure of the samples was characterized by XRD (Figure 2a), where the patterns before and after the KOH treatment are presented. It was found that the as-deposited samples were amorphous (see Figure S1 in S.I.), but a thermal annealing at 400 °C in air led to the formation of the monoclinic phase of $BiVO_4$

(JCPDS data sheet of 14-0688, space group *I2/a*, *a*=5.195 A°, *b*=11.701 A°, *c*=5.092 A°, **β**=90.38°).

Figure 2b shows the UV-Visible spectroscopy analyses, which provide details regarding the absorbance spectrum of the $BiVO_4$ thin films. The spectrum before the KOH-treatment shows a band edge at around 500 nm, as it consists of different kinds of impurities. After the treatment with KOH, the spectrum shows a red shift of band edge to higher wavelength of around 533 nm, and it refers to the intrinsic nature of monoclinic $BiVO_4$.[25] From such band edge positions, the band gap of the materials before and after the treatment was found to be about 2.48 and 2.32 eV, respectively.

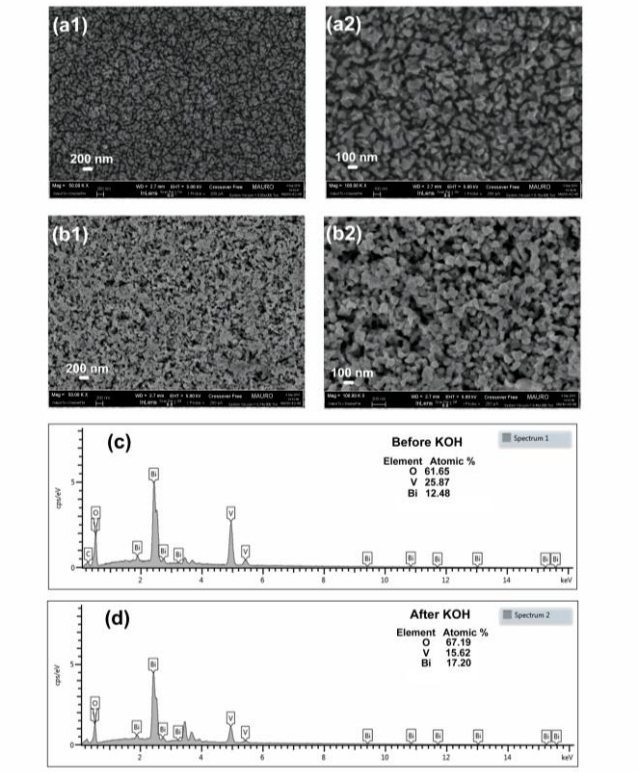

Fig 3 FESEM analysis for the $BiVO_4$ film "before" (a1,a2) and "after" (b1,b2) the KOH-treatment. EDS analysis of the $BiVO_4$ films "before" (c) and "after" the KOH-treatment. Scale bars of (a1,b1): 200 nm and of (a2,b2): 100 nm.

Figures 3 (a-b) provide details of the FESEM characterizations of the samples, in order to have an understanding of the morphology changes due to the KOH treatment. The image provides the details of the samples without (a1,a2) and with (b1,b2) the KOH treatment. It should be noted that KOH increased the sample porosity. Although the effect of the KOH treatment was not so evident from XRD analysis, the FESEM images indicates that formation of porous structure by removing the unwanted excess impurities over and around the monoclinic $BiVO_4$ grains, thus improving the surface exposure of the films.

The EDS analysis in Figures 3c and d gives information on the bulk elemental analysis of the thin films before and after the KOH treatment, respectively. The composition of the films after the chemical treatment with KOH was almost in agreement with the equimolar bismuth to vanadium ratios present in the $BiVO_4$. Meanwhile, the EDS analysis before the treatment showed an excess of V probably segregated into the grain boundaries and that was removed by the chemical treatment using KOH. The use of KOH to preferentially remove excess of V from V-rich $BiVO_4$ films have also been reported for dip-coated or electrochemical deposited films.[4, 26] Interestingly, for the sputtered $BiVO_4$ films, the KOH creates an open structure which suggests that it preferentially attacks the grain boundaries, although the whole thickness was also reduced, as described later. The formation of this porous structure has the advantage of increasing the interfacial area between the electrolyte and the film, compared to a non-porous structure.[27] The photo-generated holes will have to migrate less bulk material, in order to reach the solution interface, and thus the probability of recombining before participating in the electrochemical reaction reduces. This particular characteristic of the photo-electrode provides an additional feature that can improve the water splitting efficiency.[28] In fact, porosity in general has a benefit on the catalytic behavior of the sample since it increases the number of exposed catalytic sites. The thickness of the samples before and after the KOH treatment was measured using a profilometer, and it was observed that it decreased from around 400 nm (before) to 280 nm after the KOH treatment (see Figure S2 in the S.I). Such thickness decrement could also improve the photocurrent as has been reported by Chen *et al*.[19] Although, we did not observe it for films deposited at different deposition times, but only by the KOH treatment.

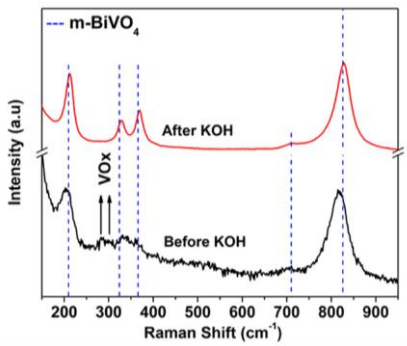

Fig 4 Raman spectroscopy for $BiVO_4$ films before the KOH-treatment (black curve), showing few peaks that correspond to vanadium oxide, and after treating the as-annealed $BiVO_4$ films with KOH (red curve), showing all the peaks of monoclinic $BiVO_4$.

Raman spectroscopy can provide structural information and is also a sensitive method for the investigation of the crystallization, local structure and electronic properties of materials. Figure 4 shows the Raman spectra of the thin films before and after the KOH treatment. The Raman spectra of the non-treated film show only two peaks from the monoclinic $BiVO_4$; the peak centered around 201 cm^{-1} and the vibrational mode of the V-O bond centered at around 826 cm^{-1}. On the other hand, two other peaks centered at ~ 282, and 306 cm^{-1} confirmed the presence of vanadium oxide impurities.[29, 30] After the KOH treatment, a perfect match of the Raman spectrum with the monoclinic $BiVO_4$ was observed, compared with the RRUFF database of the Raman spectroscopy. Indeed, Raman bands of ~ 210, 324, 366, 710, and 826 cm^{-1}, which are the typical vibrational bands of $BiVO_4$, were observed for this thin film.[31]The structural information of $BiVO_4$ is obtained from the band centered at 210 cm^{-1}. The asymmetric and symmetric formations of the VO_4 tetrahedron are given by the bands centered at 324 and 366 cm^{-1}, respectively. The stretching modes of the two vibrational modes of the V−O bonds are

determined from the bands centered at 710 and 826 cm^{-1}.[10, 25]

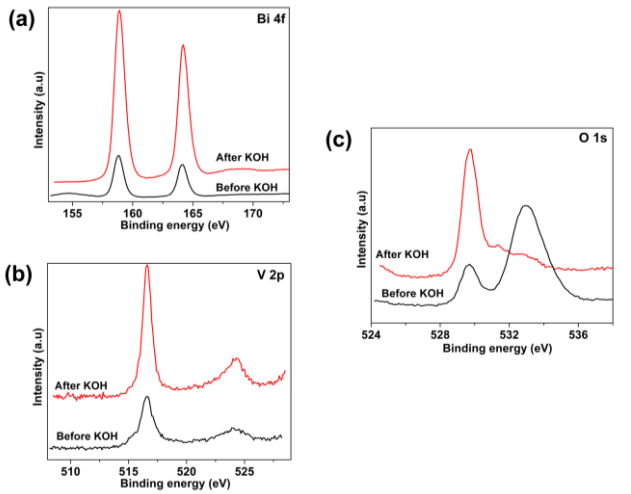

Fig 5 XPS spectra of $BiVO_4$ films before and after KOH treatment: (a) Bi 4f (b) V2p and (c) O1s

Figure 5 shows the X-ray photoelectron spectroscopy of the thin monoclinic $BiVO_4$ films before and after the KOH treatment, indicating the chemical states on the surface. The C1s peak at 284.6 eV was used for calibration purposes. Before and after the KOH-treatment: the two main asymmetric peaks, $Bi4f_{7/2}$ and $Bi4f_{5/2}$ are observed at 158.88 and 164.23 eV, respectively (see Figure 5a), while the asymmetric $V2p_{3/2}$ peak can be observed at a binding energy of 516.5 eV (see Figure 5b). Before the KOH-treatment, a high intensity of the O1s peak around 533 eV can be observed in Figure 5c, which most probably arises from either oxygen vacancies or adsorbed oxygen species (O^- and O^{2-}).[25, 32] In fact, after the KOH treatment, the O1s spectra evidenced a sharp peak at around 529.74 eV and small peaks at around 531 to 533 eV. These peaks represent the lattice oxygen (O_{latt}) (V−O) and the adsorbed oxygen (O_{ads}) species on the surface of the thin film, respectively.

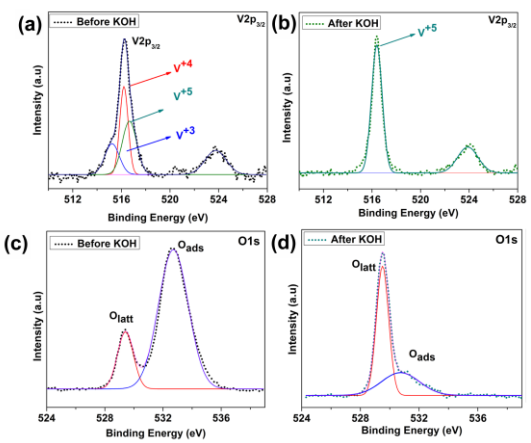

Fig 6 De-convolution spectra of V2p (a,b) and O1s (c,d) for $BiVO_4$ films before and after the KOH treatment.

Figure 6a shows that the thin films before the treatment had different levels of Vanadium oxide contamination. The presence of V^{+3}, V^{+4} and V^{+5} at 515.2 eV,[33] 516.2 eV[34] and 516.5eV,[35] respectively, is evident from the de-convoluted $V2p_{3/2}$ peak. The distribution of the V^{+5}:V^{+4}:V^{+3} ratios from the areas was found to be 39:36:25. The vanadium oxide impurities result in the film due to remains of vanadium after the formation of monoclinic $BiVO_4$ phase during the annealing at 400 °C. Hence, there should be a large number of oxygen vacancies, which are induced by the V^{+4} and V^{+3}. These oxygen vacancies, having positive charges, tend to interact with the negative charges on the surface, such as O^- and O^{2-} that arise from the atmosphere and because of the thermal treatment conditions that were employed. After the KOH treatment, the $V2p_{2/3}$ peak seems to be symmetric (see Figure 6b), but it is possible to have some traces of V^{+4} impurities in the $BiVO_4$ film throughout the thickness. The treated film hence shows fewer adsorbed O^- and O^{2-} species than the untreated film. From Figure 6c and d, the O_{latt} :O_{ads} ratio before the treatment was found to be around 18:82, which is greatly decreased to 65:35 after the KOH treatment.

Photocatalytic activity

The photo-catalytic activity of the $BiVO_4$ films was evaluated by using them as anodes for the photo-electrochemical water splitting reaction. Figure 7a shows the LSV curves of the photo-electrodes acquired under AM1.5 G illuminations, where the current density is a function of the applied potential in the PEC system. In general, the current density remains negligible until the water oxidation onset potential is reached: this potential represents the thermodynamic limit value beyond which water electrolysis occurs.

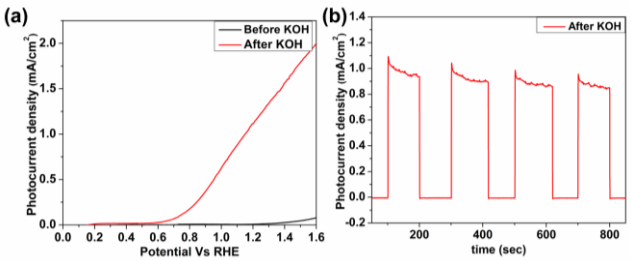

Fig 7 (a) Photocurrent-potential curves at a scan rate of 20 mV/s: before and after the KOH-treatment and (b) chrono-amperometric measurement at 0.6V *vs* Ag/AgCl of the sample after the KOH treatment. Both measurements were carried out in 0.1M Na_2SO_4 electrolyte.

The curves are characterized by an onset potential well below 1.23 V, which represents the minimum voltage that should be applied to obtain cold water dissociation in dark conditions: [36, 37] this feature highlight the photo-catalytic activity of the fabricated films. The maximum photocurrent obtained with the $BiVO_4$ thin film treated with KOH, which was synthesized under given conditions (see materials and methods), was 1.19 mA/cm^2 at 1.23 V *vs* RHE (Figure 7a). Among several possible synthesis methods, such photocurrent density produced by the $BiVO_4$ electrode gives to the synthesis procedure and treatment here reported a unique importance. In fact, the KOH treatment, on the as-annealed thin films produced by DMS, induces the formation of a more porous structure, by removing the unwanted material from the surface as well as around the grain boundaries of the monoclinic $BiVO_4$ crystals, thus increasing the number of catalytic sites, which in turn improves the photo-current density by 120 folds. Indeed, the photocurrent reported here is among the best values for $BiVO_4$ photo-electrode systems as summarized by Park et al.[4] in 2013, even without the use of co-catalysts or doping. Moreover, the

above mentioned sputtering technique has many advantages over other thin film synthesis techniques, as it is an industrially scalable and reliable technique for the production of thin films with homogenous and continuous surfaces.

Similarly, figure 7b represents the chrono-amperometric measurements, which were performed in order to check the stability of the $BiVO_4$ photoanode and have revealed that the current density was stable for a long period of time. In fact, the *I-t* curves show good photocurrent stability under numerous ON-OFF light cycles. The charge transfer and transport mechanisms that occur in the $BiVO_4$ thin films before and after the KOH treatment were carefully analyzed by means of electrochemical impedance spectroscopy (EIS) technique, in order to obtain a better understanding of the electrodes behavior, as reported in the following section.

Electrochemical Impedance Spectroscopy

EIS is a well-known technique that is often employed to characterize electrochemical systems and devices for different kinds of applications,[38] including photo-electrochemical water splitting.[39]

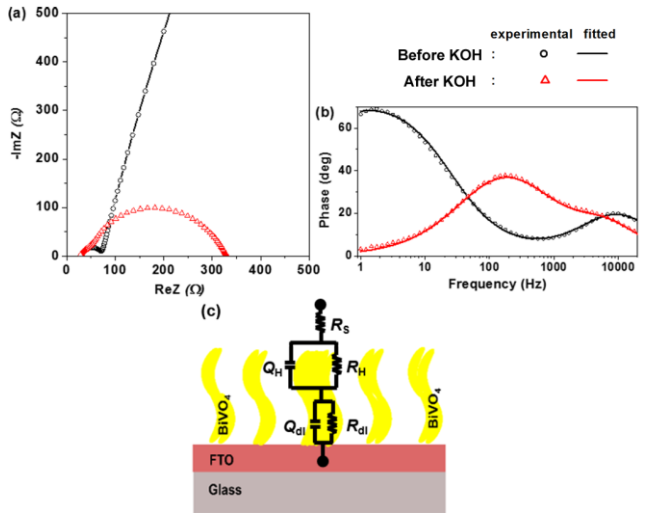

Fig 8 (a) Bode and (b) Nyquist plots of impedance of the $BiVO_4$ electrodes before and after the KOH treatment, at 1.23V *vs* RHE under AM1.5G simulated sunlight in Na_2SO_4(0.1M) electrolyte.(c) Equivalent circuit used to fit EIS data and schematic representation of thin film structure.

Figure 8 shows the results of Electrochemical Impedance Spectroscopy (EIS) measurements made with an applied DC potential of 0.6 V *vs* Ag/AgCl under AM1.5G simulated sun-light condition (at 1 sun). In the Nyquist plots in Figure 8a, a wide semi-circle at low frequencies and a small semi-circle at high frequencies are observed, which can be correlated with both structural and photocatalytic properties of the films. In accordance with the LSVs, the impedance of the non-treated $BiVO_4$ electrode is higher than that of the KOH treated material, which in turn corresponds to a decrease in the number of electrons transferred through the electrode/electrolyte interface.[40] Moreover, from the Bode diagram in Figure 8b (phase *vs* frequency) two features can be recognized, related to the two different processes occurring in the analyzed electrodes: a high frequency peak (above 1000 Hz), associated with the charge transport properties in the bulk of the photo-electrode materials, and a low frequency peak (between 1 and 1000 Hz) associated with the charge transfer at the photo-electrode/electrolyte interface.[41] In order to evaluate the time constants associated with such two processes, EIS spectra were modeled by using the equivalent circuit (EC) shown in Figure 8c.[38, 42, 43] This EC has been previously used to evaluate the different charge transport phenomena occurring at n-type semiconductors and other porous materials:[38, 39, 42, 44] R indicates a resistance and Q is a constant phase elements (CPE), representing a non-ideal capacitance associated with a non-uniform current distribution in heterogeneous materials. The impedance of a CPE is defined as:

$$Z_{CPE} = \frac{1}{(j\omega)^n Q} \quad (1)$$

where n ($0 < n < 1$) is the CPE index.[44] The lower is *n*, the higher is the roughness associated with the electrode surface. The capacitance associated with the CPE is given by:

$$C = Q^{(1/n)} R^{((1/n)-1)} \quad (2)$$

In particular, R_s is the series resistance, which comprise the FTO film, the external electrical contacts and the liquid electrolyte. The two parallels R//Q correspond to the two distinct charged regions induced in semiconductor electrodes during the electrochemical processes: (i) the Helmholtz double layer formed at the $BiVO_4$/electrolyte interface (related to R_H//Q_H) and (ii) the depletion layer in the semiconductor side,[39, 42] across which a potential gradient exists (related to R_{dl}//Q_{dl}). The time constants corresponding to the transport and transfer of charge carriers in such regions can be calculated through the expression:

$$\tau = R \cdot C \quad (3)$$

By comparing the markers and the continuous lines in Figure 8 is evident that the fitted data agree very well with the experimental one. The charge transport time constant (τ_{dl}) in both the $BiVO_4$ films remained of the same order of magnitude after the KOH treatment (*i.e.* $2.8*10^{-2}$ and $3.3*10^{-2}$ ms, for the non-treated and the treated samples, respectively). Such values also agree with the similar position of the phase peak in the high frequency region for both samples and confirm that the KOH treatment does not alter the bulk properties of the $BiVO_4$ electrode. On the other hand, the time constant related to the charge transfer at the Helmholtz double layer (τ_H) resulted to be about 2.2 s for the non-treated $BiVO_4$ film and 3.2 ms for the KOH treated $BiVO_4$ one. Such means that the KOH treatment was able to improve the charge transfer, and thus the kinetics of the photocatalytic water oxidation, by fastening the reaction by three orders of magnitude, as it was already evidenced by the current-potentials curves in Figure 7a. Such result is also evident from the shift of the phase peak of the Bode plot from about 2 Hz up to about 200 Hz, and the related reduction on the charge transfer resistance from about 11200 to 280 Ω/cm^2, before and after the KOH treatment, respectively. This noteworthy result is in-line with the hypothesis that after the $BiVO_4$ synthesis by DMS and annealing, some non-active vanadium oxide was also formed in the film surface thus reducing the reactivity of the monoclinic $BiVO_4$, which in turn remains totally exposed after the KOH treatment. In addition, it is important to highlight that the CPE index at the electrode/electrolyte interphase (n_H), which decreased from 0.86 to 0.79 after the KOH treatment, indicates a relative

increase in the porosity of the material,[38, 42]. This result further confirms the porous nature of the KOH treated $BiVO_4$ film prepared by the DMS procedure and supports the increase of its effective roughness (*i.e.* porosity and effective active area) after the removal of the superficial non active species.

Conclusions

In this work, DMS and a post treatment for the as-annealed samples with KOH have successfully been implemented for the synthesis of thin and porous $BiVO_4$ films with monoclinic scheelite-like phase. The stoichiometric ratio of the individual elements of the $BiVO_4$ layer was obtained by means of a treatment with a 1M KOH solution, as confirmed by EDS, XPS, and Raman analysis. The charge transport and transfer properties of the $BiVO_4$ film have been analyzed by using EIS, and the photo-electrochemical performance has been assessed by LSVs and amperometric measurements. It has been observed that the thin $BiVO_4$ film produced a photo-current density of 1.19 mA/cm^2 at a bias voltage of 1.23 V *vs* RHE under AM1.5G simulated sunlight maintained at 1 sun. Future works are in progress for further modifications (doping, co-catalyst addition, etc) of the $BiVO_4$ thin films in order to improve their water oxidation capabilities.

Notes and references

The authors would like to thank Prof. Alberto Tagliaferro for his valuable discussions. Thankfulness for the European commission projects: PHOCSCLEEN (FP7) and Eco^{2}CO$_2$ (FP7) for financial support (Grant numbers 318977 and 309701). Thanks to Raimondo Mauro and Omar Novelo for the FESEM analysis and Adriana Tejeda for the XRD analysis.

[a] *Department of Applied Science and Technology, Politecnico di Torino, Corso Duca degli Abruzzi 24, 10129 Torino, Italy.;*
[b] *Instituto de Investigaciones en Materiales, Universidad Nacional Autónoma de México, Circuito Exterior s/n CU, México D.F. 04510, Mexico;*
[c] *Center for Space Human Robotics (IIT@POLITO), Istituto Italiano di Tecnologia, Corso Trento 21, 10129, Torino, Italy.*
** Fax: +39-011-0904624 Tel: +39-011-0904774; E-mail: sitaramanjaneya.thalluri@polito.it*

1. T. Hisatomi, J. Kubota and K. Domen, *Chem Soc Rev*, 2014, 43, 7520-7535.
2. R. Abe, *J Photoch Photobio C*, 2010, 11, 179-209.
3. A. Kudo, *J Ceram Soc Jpn*, 2001, 109, S81-S88.
4. Y. Park, K. J. McDonald and K. S. Choi, *Chem Soc Rev*, 2013, 42, 2321-2337.
5. F. E. Osterloh, *Chem Soc Rev*, 2013, 42, 2294-2320.
6. Z. F. Huang, L. Pan, J. J. Zou, X. W. Zhang and L. Wang, *Nanoscale*, 2014, 6, 14044-14063.
7. Y. Q. Liang and J. Messinger, *Phys Chem Chem Phys*, 2014, 16, 12014-12020.
8. J. Y. Gan, X. H. Lu and Y. X. Tong, *Nanoscale*, 2014, 6, 7142-7164.
9. A. Iwase and A. Kudo, *J Mater Chem*, 2010, 20, 7536-7542.
10. G. M. Wang, Y. X. Ling, X. H. Lu, F. Qian, Y. X. Tong, J. Z. Zhang, V. Lordi, C. R. Leao and Y. Li, *J Phys Chem C*, 2013, 117, 10957-10964.
11. Q. X. Jia, K. Iwashina and A. Kudo, *P Natl Acad Sci USA*, 2012, 109, 11564-11569.
12. W. J. Luo, Z. S. Yang, Z. S. Li, J. Y. Zhang, J. G. Liu, Z. Y. Zhao, Z. Q. Wang, S. C. Yan, T. Yu and Z. G. Zou, *Energ Environ Sci*, 2011, 4, 4046-4051.
13. R. Saito, Y. Miseki and K. Sayama, *Chem Commun*, 2012, 48, 3833-3835.
14. S. Hernández, S. M. Thalluri, A. Sacco, S. Bensaid, G. Saracco and N. Russo, *Applied Catalysis A: General*, DOI: http://dx.doi.org/10.1016/j.apcata.2015.01.019.
15. E. Alarcon-Llado, L. Chen, M. Hettick, N. Mashouf, Y. J. Lin, A. Javey and J. W. Ager, *Phys Chem Chem Phys*, 2014, 16, 1651-1657.
16. L. Chen, E. Aarcon-Lado, M. Hettick, I. D. Sharp, Y. J. Lin, A. Javey and J. W. Ager, *J Phys Chem C*, 2013, 117, 21635-21642.
17. S. P. Berglund, D. W. Flaherty, N. T. Hahn, A. J. Bard and C. B. Mullins, *J Phys Chem C*, 2011, 115, 3794-3802.
18. S. P. Berglund, A. J. E. Rettie, S. Hoang and C. B. Mullins, *Phys Chem Chem Phys*, 2012, 14, 7065-7075.
19. L. Chen, F. M. Toma, J. K. Cooper, A. Lyon, Y. Lin, I. D. Sharp and J. W. Ager, *ChemSusChem*, 2015, 8, 1066-1071.
20. K. P. S. Parmar, H. J. Kang, A. Bist, P. Dua, J. S. Jang and J. S. Lee, *Chemsuschem*, 2012, 5, 1926-1934.
21. J. A. Seabold and K. S. Choi, *J Am Chem Soc*, 2012, 134, 2186-2192.
22. F. F. Abdi, N. Firet and R. van de Krol, *Chemcatchem*, 2013, 5, 490-496.
23. L. H. Han, F. F. Abdi, P. P. Rodriguez, B. Dam, R. van de Krol, M. Zeman and A. H. M. Smets, *Phys Chem Chem Phys*, 2014, 16, 4220-4229.
24. A. S. Bondarenko and G. A. Ragoisha, *Progress in Chemometrics Research*, Nova Science Publication, New York, A. L. Pomerantsev (Ed.) edn., 2005.
25. S. M. Thalluri, C. M. Suarez, S. Hernandez, S. Bensaid, G. Saracco and N. Russo, *Chem Eng J*, 2014, 245, 124-132.
26. J. A. Seabold, K. Zhu and N. R. Neale, *Phys Chem Chem Phys*, 2014, 16, 1121-1131.
27. M. Zhou, J. Bao, Y. Xu, J. J. Zhang, J. F. Xie, M. L. Guan, C. L. Wang, L. Y. Wen, Y. Lei and Y. Xie, *Acs Nano*, 2014, 8, 7088-7098.
28. L. Dong, X. F. Zhang, X. L. Dong, X. X. Zhang, C. Ma, H. C. Ma, M. Xue and F. Shi, *J Colloid Interf Sci*, 2013, 393, 126-129.
29. V. G. Pol, S. V. Pol, J. M. Calderon-Moreno and A. Gedanken, *J Phys Chem C*, 2009, 113, 10500-10504.
30. Y. M. Li, S. D. Ji, Y. F. Gao, H. J. Luo and M. Kanehira, *Sci Rep-Uk*, 2013, 3.
31. S. Obregon and G. Colon, *Catalysis Science & Technology*, 2014, 4, 2042-2050.
32. X. Zhang, J. Qin, Y. Xue, P. Yu, B. Zhang, L. Wang and R. Liu, *Sci Rep-Uk*, 2014, 4, Article number: 4596.
33. J. Mendialdua, R. Casanova and Y. Barbaux, *J Electron Spectrosc*, 1995, 71, 249-261.
34. G. A. Sawatzky and D. Post, *Phys Rev B*, 1979, 20, 1546-1555.
35. S. M. Thalluri, M. Hussain, G. Saracco, J. Barber and N. Russo, *Ind Eng Chem Res*, 2014, 53, 2640-2646.
36. A. Kudo and Y. Miseki, *Chem Soc Rev*, 2009, 38, 253-278.
37. J. Y. Kim, G. Magesh, D. H. Youn, J.-W. Jang, J. Kubota, K. Domen and J. S. Lee, *Sci. Rep.*, 2013, 3.
38. X. Dominguez-Benetton, S. Sevda, K. Vanbroekhoven and D. Pant, *Chem Soc Rev*, 2012, 41, 7228-7246.
39. T. Lopes, L. Andrade, H. A. Ribeiro and A. Mendes, *International Journal of Hydrogen Energy*, 2010, 35, 11601-11608.
40. N. Mahato and M. Singh, *Portugaliae Electrochimica Acta*, 2011, 29, 233-251.
41. S. Hernandez, D. Hidalgo, A. Sacco, A. Chiodoni, A. Lamberti, V. Cauda, E. Tresso and G. Saracco, *Phys Chem Chem Phys*, 2015, 17, 7775-7786.
42. D. Hidalgo, R. Messina, A. Sacco, D. Manfredi, S. Vankova, E. Garrone, G. Saracco and S. Hernandez, *International Journal of Hydrogen Energy*, 2014, 39, 21512-21522.
43. S. Hernandez, M. Tortello, A. Sacco, M. Quaglio, T. Meyer, S. Bianco, G. Saracco, C. F. Pirri and E. Tresso, *Electrochim Acta*, 2014, 131, 184-194.
44. E. Barsoukov and J. R. Macdonald, *Impedance Spectroscopy: Theory, Experiment, and Applications*, Wiley, 2 edn., 2005.

An overview of the sputtering procedure, the chemical treatment involved to produce porous $BiVO_4$ film and its activity.

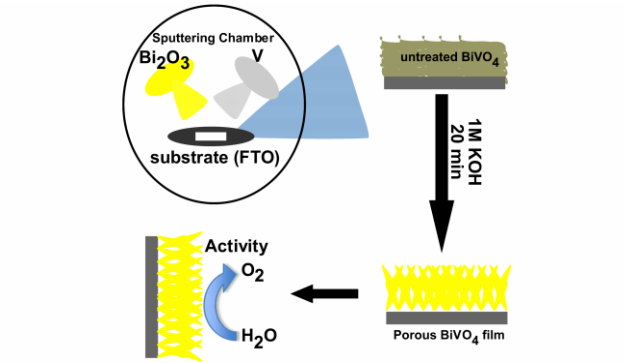

TOC Figure